Self-assembled clusters of spheres related to spherical codes

Carolyn L. Phillips,[1,*] Eric Jankowski,[2,†] Michelle Marval,[3] and Sharon C. Glotzer[1,2,3,‡]
[1]*Applied Physics Program, University of Michigan, Ann Arbor, Michigan, 48109, USA*
[2]*Department of Chemical Engineering, University of Michigan, Ann Arbor, Michigan, 48109, USA*
[3]*Department of Materials Science and Engineering, University of Michigan, Ann Arbor, Michigan, 48109, USA*
(Received 15 January 2012; revised manuscript received 2 August 2012; published 15 October 2012)

We consider the thermodynamically driven self-assembly of spheres onto the surface of a central sphere. This assembly process forms self-limiting, or terminal, anisotropic clusters (N-clusters) with well-defined structures. We use Brownian dynamics to model the assembly of N-clusters varying in size from two to twelve outer spheres and free energy calculations to predict the expected cluster sizes and shapes as a function of temperature and inner particle diameter. We show that the arrangements of outer spheres at finite temperatures are related to spherical codes, an ideal mathematical sequence of points corresponding to the densest possible sphere packings. We demonstrate that temperature and the ratio of the diameters of the inner and outer spheres dictate cluster morphology. We present a surprising result for the equilibrium structure of a 5-cluster, for which the square pyramid arrangement is preferred over a more symmetric structure. We show this result using Brownian dynamics, a Monte Carlo simulation, and a free energy approximation. Our results suggest a promising way to assemble anisotropic building blocks from constituent colloidal spheres.

DOI: 10.1103/PhysRevE.86.041124 PACS number(s): 64.60.De, 02.70.Ns, 47.57.J−

I. INTRODUCTION

Anisotropic particles are compelling building blocks for self-assembled materials because their directional interactions can be exploited to create complicated and useful patterns [1–7]. One way to create anisotropic building blocks is to self-assemble them from simpler particles, resulting in terminal building blocks that represent free energy minimizing structures (Fig. 1). Perhaps the simplest building block is the colloidal sphere, which can be synthesized from a wide variety of polymers and metals, and the interactions between which can be tuned with great precision through the choice of solvents, salts, and organic ligands [8–11]. A variety of compound building blocks composed of spheres have been recently synthesized [12–16] and studied computationally [6,17–22].

Here we consider a class of self-limiting, or "terminal", colloidal clusters created by the self-assembly of one type of particle, the "halo" particle (HP), around a second type of particle, the central particle (CP). The clusters are terminal because the only interparticle attraction is between the HP and CP, which are dilute in the fluid of HP, and therefore steric restrictions among co-adsorbed HPs inhibit further growth. The resulting clusters have structures determined by the interactions among the adsorbed HPs. Furthermore, the HPs are assumed to be able to diffuse freely on the CP surface without desorbing, constrained only by their interactions with other HPs. Thus the HP can self-organize around the CP to minimize their free energy. We investigate the self-assembly of these clusters as a function of particle diameter and temperature in a semi-open system, where balance between HP binding energy and entropy controls the equilibrium clusters observed. The arrangements of HPs bear comparison to a particular set of solutions, the *spherical codes* [23–26], for certain ratios of particle diameters. In addition to providing a way to synthesize anisotropic clusters, this assembly approach can be used to template patchy spherical particles or nanoparticle cages (Fig. 1). These clusters also resemble the complex self-assembled lock-and-key colloidal "molecules" experimentally created by Sacanna *et al*. [27].

This paper is organized as follows: In Sec. II, we introduce the methods we use to study the terminal N-clusters, including Brownian dynamics (BD) simulations, Monte Carlo simulations (MC), and free energy calculations. In Sec. III, we report the results of our simulations and free energy calculations. We find that terminal N-clusters self-assemble across a range of diameters and temperatures. These findings are supported by our free energy calculations, which predict cluster sizes and probability distributions. In Sec. IV we introduce spherical codes and show that the structures of the self-assembled clusters resemble spherical code solutions. In Sec. V, by using BD simulations and free energy calculations, we explain the surprising observation of a dominant low-symmetry $N = 5$ cluster, a deviation from the spherical code prediction. In Sec. VI, we discuss several ways that this work can be extended to create more types of anisotropic particles via tuning of the particle interactions, constructing additional shells of particles, and creating structurally reconfigurable particles. In Sec. VII we conclude with a summary of our findings.

II. METHODS

To predict and compare the terminal N-clusters of halo particles bonded to central particles we use computational tools that sample equilibrium statistical mechanical ensembles. We performed computer experiments of the self-assembly of model particles and the results of these simulations are compared against cluster probabilities calculated from a free energy analysis based upon numerical partition function calculations [7].

*Present address: Computation Institute, Argonne National Laboratory, Lemont, Illinois, USA.
†Present address: University of Colorado at Boulder, Boulder CO 80309.
‡sglotzer@umich.edu

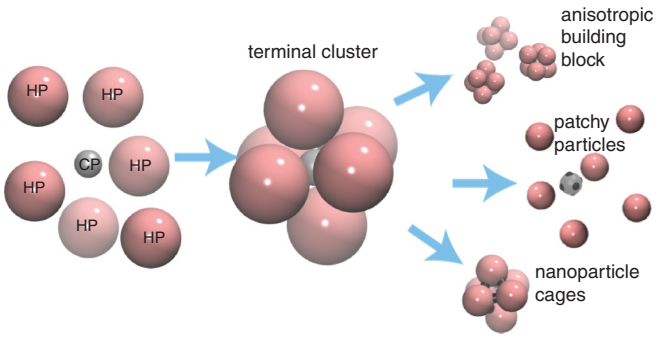

FIG. 1. (Color online) A terminal N-cluster with octahedral structure ($N = 6$) self-assembled from a bath of HP and a CP. This cluster has applications as an anisotropic building block, and could be used to manufacture a "patchy particle" by imparting patches on the CP at the contact points, or could be locked into a nanocolloidal cage structure.

A. Hard sphere and sticky sphere model

We wish to model hard colloidal spheres adsorbed onto a sticky sphere of a different diameter. Mathematically, perfectly hard spheres are points interacting via a function that steps from infinity to zero and perfectly sticky spheres are points interacting via the same function plus an infinitely narrow square well function. Given HPs of diameter D_h and a CP of diameter D_c, the interaction potential between ideal HPs is defined as

$$U_{H-H}(r) = \begin{cases} \infty, & r < D_h \\ 0, & r \geqslant D_h, \end{cases} \tag{1}$$

and the interaction potential between an ideal HP and an ideal CP is defined as

$$U_{H-C}(r) = \begin{cases} \infty, & r < (D_c + D_h)/2 \\ -E_0, & r = (D_c + D_h)/2 \\ 0, & r > (D_c + D_h)/2. \end{cases} \tag{2}$$

The nondimensional ratio of the diameters is then defined as $\Lambda = D_c/D_h$.

We use several types of computer experiments to study the assembly of clusters and the stability of already assembled clusters. To collect sufficient statistics for a wide range of Λ and at different temperatures, we use BD simulations, and radially shifted Weeks-Chandler-Andersen (WCA) and Morse models of hard and sticky spheres, respectively. To study already assembled athermal clusters with mathematically ideal potentials at specific values of Λ, we use MC simulations.

The BD simulations are computationally efficient. The potentials used capture, in a general sense, the repulsive and attractive interactions of the constituent particles. However, insofar as the potentials used are not the mathematically ideal potentials, careful accounting of the softness of the particles and width of the potential well is necessary to compare results to ideal mathematical predictions. We note that an experimental realization of this system also will need to perform a similar careful accounting [28]. The details of the BD simulations are discussed in the Supplemental Material (SM) §1–5 [29]. When results are generated by a BD simulation, the results will be shown as a function of Λ^{BD} to indicate this.

In general, good agreement was found between the BD and MC simulations. From this we conclude that, qualitatively, our results are independent of the details of the model potentials used and that the universal aspects of our results should be observable in experimental systems that also deviate from the mathematical ideal. As nanoparticle synthesis continues to mature, the types of interactions that can be used to guide the self-assembly of small particles can be precisely tuned over wide ranges of length and energy scales, and the models used in BD simulations can be suitably adjusted to match the experimental systems.

B. Free energy calculations

The relative probability of finding a particular cluster of N HPs bound to a CP can be predicted using free energy calculations detailed in Refs. [7,22,30]. For a given Λ, the partition function is defined by the appropriately weighted sum over all possible configurations of N HPs bound to a CP for $N = 1$ to ∞. The contributions of the distinguishable microstates to the partition function are calculated numerically.

The partition function is calculated assuming ideal hard spheres and sticky spheres as per Eqs. (1) and (2). To vary Λ, D_h is held constant and set to $D_{h,e}$ of the SM §2 [29], and D_c is varied.

If, for a given Λ, M is the maximum number of HP that can be bonded to the CP, then configurations of M HPs bonded to the CP minimize the potential energy and configurations with more than M HPs have infinite potential energy (zero probability). Configurations with fewer than M HPs bonded to the CP increase the entropy of the cluster. When $k_BT \approx E_0$, the free energy can be minimized by clusters with fewer than M HPs, because the entropy gained by the remaining HPs on the CP balances the potential energy associated with removing a HP. In the grand canonical ensemble, at a fixed Λ, the probability of observing a particular cluster s is given by the Boltzmann distribution:

$$P_s = e^{-\beta F_s} = \frac{\Omega_s e^{-\beta(U_s - \mu N)}}{\mathcal{Z}}, \tag{3}$$

where $\mathcal{Z} = \sum_s \Omega_s \exp[-\beta(U_s - \mu N)]$ is the partition function and $U_s - \mu N = N E_0$. Without loss of generality, we treat $\mu = 0$. (A nonzero μ will only induce a uniform temperature shift in our final results.)

In practice, calculating $\mathcal{Z}$ exactly is difficult, but by assuming that only a small number of clusters contribute to $\mathcal{Z}$ [7,22,30], the relative probabilities of these clusters can be determined. As in Refs. [7,22,30], the degeneracy Ω_s can be written as a product of three independent terms: the translational Z_t, rotational Z_r, and vibrational Z_v partition functions. The translational partition function is approximately equal for all the clusters because they are all small compared to the accessible volume, and thus it contributes equally to the Ω_s of each cluster.

To calculate the rotational and vibrational partition functions for an N-cluster, we first assume an equilibrium configuration defined by N HPs at the spherical coordinates of the densest possible configuration (described in detail in

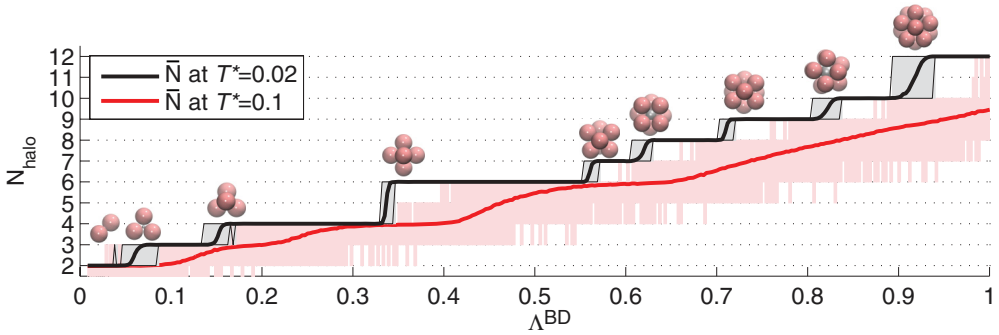

FIG. 2. (Color online) N clusters that self-assemble as a function of Λ^{BD} and temperature. The average N of the self-assembled cluster at $T^* = 0.02$ is shown as a black line. The maximum and minimum N in the simulation is shaded gray. The average N of the self-assembled cluster at $T^* = 0.1$ is a red solid line. The maximum and minimum N in the simulation is shaded pink. Example clusters self-assembled in simulation are shown above the black line near the Λ^{BD} at which they are first observed.

Sec. IV) at a radial displacement of $(D_c + D_h)/2$ from the CP. The rotational partition function is then calculated as $Z_r = c_r N! \sqrt{I}/\kappa$, where c_r is a temperature-dependent constant that is the same for all the clusters, I is the determinant of the moment of inertia tensor, and κ is the symmetry number of the densest configuration under rotation. Each sphere is given a unit mass. The vibrational partition function is proportional to the product of the free volumes of each sphere in the cluster. The free volume of a particle is an important thermodynamic quantity in hard sphere and disk systems [31–34] and is a measure of the vibrational freedom, or freedom to rattle. The vibrational freedom of each HP can be measured as the fractional area of the surface of the CP it has access to, subject to the restrictions imposed by its neighboring spheres. We approximate the vibrational area available to a given HP in a particular configuration by using a Monte Carlo numerical approach whereby new positions for the HP are randomly generated and accepted if the HP does not overlap another HP. The accessible vibrational area is proportional to the total number of accepted positions that are part of a contiguous area that includes the HP's original position divided by the total number of random trials. At the densest Λ, most, if not all, of the spheres in an N-cluster are jammed and have no vibrational freedom.

The free energy calculation is approximate, as it does not consider the contribution of collective modes of HP motion to $\mathcal{Z}$, which, in certain systems, can help stabilize one configuration over another [35]. We observe that each cluster has a small Λ range where collective modes are absent, and only local rattling is observed. A more detailed description of the collective modes of these clusters can be found in Ref. [36]. Outside this range, we expect some error in the calculation of relative probabilities to accumulate. The benefit of this free energy approximation is demonstrated by both its favorable comparison to predictions made by BD simulations and by its ability to rapidly predict the entire phase diagram. Applying a more computationally intensive method to perform an exact free energy comparison would be an interesting topic for future study.

III. RESULTS

Using Brownian dynamics we simulate the self-assembly of clusters as a function of Λ^{BD} and at two different temperatures, $T^* = 0.02$ (low) and $T^* = 0.1$ (high), to investigate the effect of thermal noise on the distribution of stable terminal N-clusters. We compare these results to free energy calculations.

At the low temperature we observe that the cluster sizes are highly monodisperse as a function of Λ^{BD}. In Fig. 2, the mean cluster size assembled at the low temperature, $T^* = 0.02$ for $0.01 < \Lambda^{BD} < 1$ is shown as a black solid line. Gray shading indicates the range of cluster sizes observed at a particular Λ^{BD}. Over this range of Λ^{BD} clusters are uniform in size except when Λ^{BD} is near a value where there is a transition from one mean cluster size to another. At these transitions, we observe a narrowly distributed mixture of cluster sizes; for example, at $\Lambda^{BD} = 0.71$ for the $T^* = 0.02$ curve, we find equal numbers of clusters containing 8 or 9 HPs.

In comparison to the low temperature data, the clusters at high temperature are both smaller on average and have a broader distribution of sizes as a function of Λ^{BD}. In Fig. 2, we show the distribution of clusters assembled at high temperature, $T^* = 0.1$ (red). The region shaded pink represents the range of cluster sizes measured at a given Λ^{BD} at $T^* = 0.1$. At $\Lambda^{BD} = 0.71$ for the $T^* = 0.1$ curve, we observe clusters of 5, 6, 7, and 8 HPs rather than just the clusters of $N = 8$ and 9 observed at $T^* = 0.02$. We also observe that the $N = 5$ and $N = 11$ clusters are not stable at any Λ^{BD} at low temperature but are present in the broader distribution of clusters at high temperature.

We calculate the free energies of all clusters from $N = 2$ to $N = 12$ over a temperature range of $0.02 \leqslant T^* \leqslant 0.2$ and diameter ratio range of $0.05 \leqslant \Lambda \leqslant 1.09$. In Fig. 3, we report a "phase diagram" of the most probable cluster at each combination of T^* and Λ. Figures 4 and 5 compare cluster probabilities from an in-page slice of the phase diagram with the distributions observed from BD simulations at $T^* = 0.02$ and $T^* = 0.1$.

The cluster probability distributions predicted by our free energy calculations are consistent with the distributions observed in BD simulations. This strong correspondence indicates that the single-particle vibrational freedom is the most relevant factor driving cluster structure aside from the binding energy between HP and CP. Both the BD simulations and free energy calculations show that, for a given Λ, the average cluster size decreases and the cluster size distribution broadens at higher temperature. The Λ displacement and precise shape

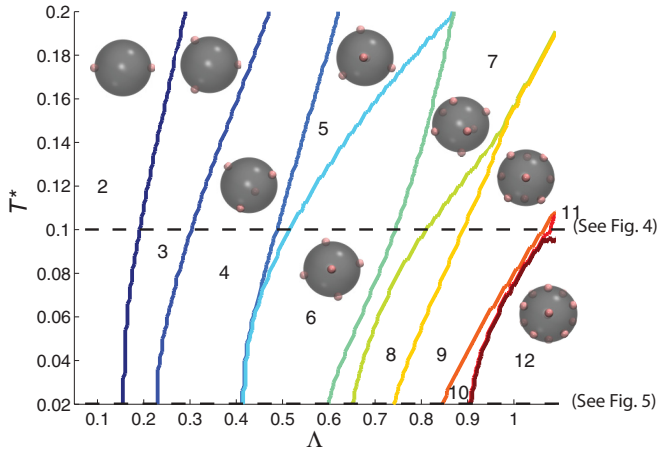

FIG. 3. (Color online) Most probable cluster size as a function of Λ and T^* from free energy calculations. Colored curves indicate state points of cluster size coexistence. For example, the teal curve indicates the values of Λ and T^* where $N = 6$ clusters are as probable as $N = 4$ or $N = 5$ clusters.

of the cluster probability distributions differ slightly between the BD simulations and free energy calculations because of the soft sphere and bonding approximation used in the BD simulations, and the collective vibrational modes that exist in the simulations but are neglected in the free energy calculations.

Consistent with the BD simulation data, the free energy calculation predicts that $N = 5$ clusters are not stable at low ($T^* < 0.06$) temperatures. This is because the densest $N = 5$ clusters occur at the same Λ as the densest $N = 6$ cluster. Thus, for $T^* < 0.06$ the free energy is dominated by the potential energy, stabilizing the $N = 6$ cluster over the $N = 5$ cluster.

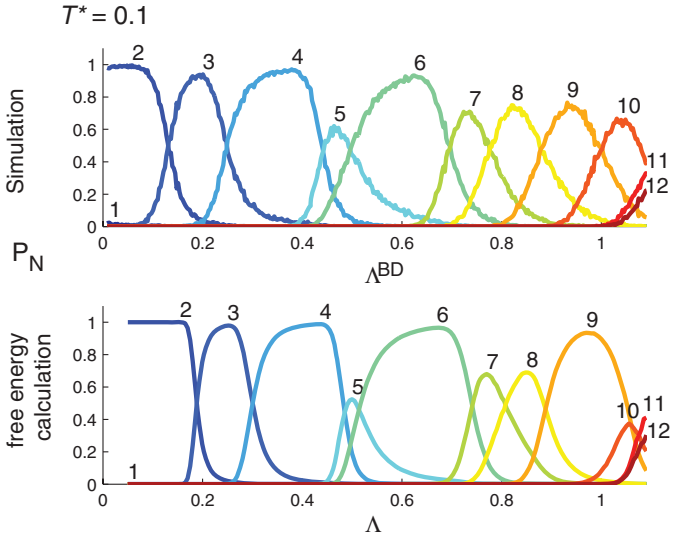

FIG. 4. (Color online) Cluster probability as a function of diameter ratio at high temperature ($T^* = 0.1$). Probabilities observed in BD simulations are plotted above, and probabilities calculated from free energy calculations are shown below. Compared to the lower temperature (Fig. 5), the cluster size distributions shown here are broader, with multiple cluster sizes coexisting over a range of Λ and Λ^{BD}.

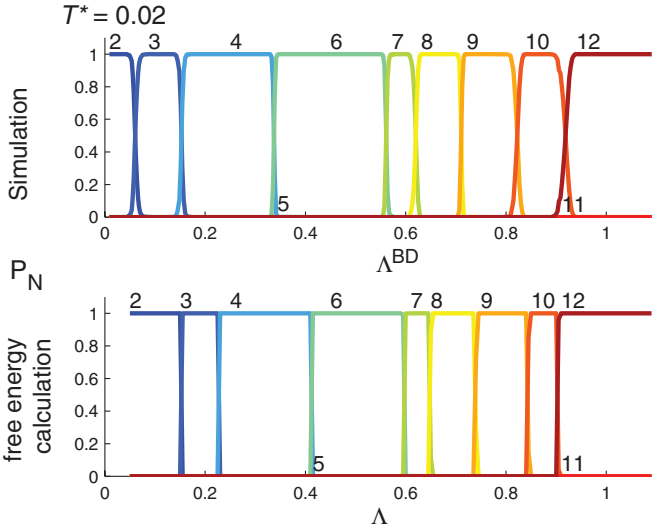

FIG. 5. (Color online) Cluster probability as a function of diameter ratio at low temperature ($T^* = 0.02$). Probabilities observed in BD simulations are plotted above, and probabilities calculated from free energy calculations are shown below. Compared to the higher temperature (Fig. 4), here we observe sharp transitions between cluster sizes as a function of Λ and Λ^{BD}.

However, the free energy calculation predicts that at $T^* > 0.06$ there is a Λ range where an $N = 5$ cluster is the most probable cluster. This Λ range is observable in the high temperature BD simulation data. The stabilization of the $N = 5$ cluster over the $N = 6$ cluster at higher T^* arises from the non-negligible contribution of the vibrational partition function, the only term in the partition function that significantly differs between the two clusters. The $N = 11$ cluster is similarly predicted to be unstable at low temperatures but stable over the $N = 12$ cluster at a higher temperature. The free energy calculation also predicts an entropic stabilization of the $N = 7$ and 9 clusters over the $N = 8$ and 10 clusters, respectively, at higher T^*, and "triple points" at which the probabilities of three clusters (e.g., 4, 5, and 6, or 7, 8, and 9) are equal.

IV. SPHERICAL CODES

The structure of the clusters self-assembled in Sec. III have a direct analog to a well-studied problem in mathematics known as the *spherical code* problem (also known as the Fejes Tóth, or Tammes problem), whose solutions are a sequences of points distributed on the surface of a sphere such that the minimum distance between any pair of points is maximized [23–26].

Figure 6 depicts the spherical code solutions for $1 \leqslant N \leqslant 12$. The arrangement of points for $N = 4$ corresponds to the vertices of a regular tetrahedron, $N = 6$ an octahedron, $N = 8$ a square antiprism, and $N = 12$ an icosahedron. The point arrangement of $N = 11$ is equal to the $N = 12$ solution minus a single point, or an icosahedron with one truncated pentagonal face (also known as a diminished icosahedron, or gyroelongated pentagonal pyramid). For each N, the point group—the group of isometries that keeps one point fixed—of the arrangement [25] is shown in the upper right corner. Each optimal arrangement of N points on the surface of the sphere is unique except for $N = 5$ which has a continuum of solutions

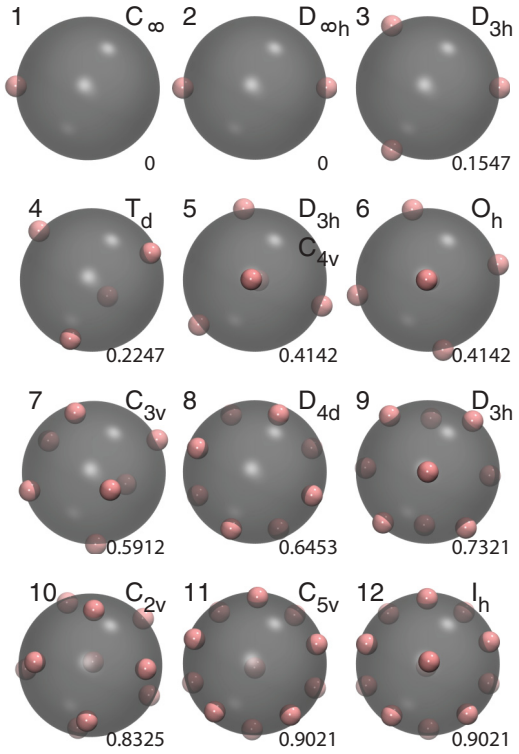

FIG. 6. (Color online) Arrangement of points (pink) that correspond to each spherical code solution for $1 \leqslant N \leqslant 12$. The point group of each arrangement is shown to the upper right of each arrangement, and the densest packing diameter ratio $D_c/D_h = \Lambda_{SC}$ is shown to the lower right. For $N = 5$, the triangular bipyramid configuration is shown. Other $N = 5$ configurations are shown and discussed in Figs. 7 and 8.

ranging from a triangular bipyramid [point group D_{3h}, shown in Figs. 6 and 8(b)] to a square pyramid [point group C_{4v}, shown in Fig. 8(a)]. All solutions in the continuum have two points at opposite poles of the central sphere and differ by the positions of the three remaining points on the equator. The square pyramid arrangement is equal to the $N = 6$ solution minus a single point.

If the N points represent sphere centers, the spherical code solution corresponds to the densest packing of N hard halo spheres that all "kiss" a central sphere. Each solution, therefore, corresponds to single value of Λ that we will denote[1] as Λ_{SC}. In Fig. 6, the Λ_{SC} of each arrangement is shown to four significant digits in the bottom right corner. In one of mathematics' most famous debates, Isaac Newton and David Gregory argued whether the kissing number of unit spheres ($\Lambda = 1$) is 12 or 13. Had it been known that a central unit sphere can only be kissed by 13 spheres if their radii is $r \leqslant 0.9165$, or $\Lambda_{SC,N=13} = 1.0911$ [24], this would have settled the question. Instead, Isaac Newton's conjecture that the kissing number is 12 was not proven until 1953 [37].

We observe that the clusters that self-assemble in Fig. 2 have the structure of the spherical code solutions. The disappearance of $N = 5$ and $N = 11$ in Figs. 2 and 3 at $T^* = 0.02$ is consistent with $\Lambda_{SC,N=5} = \Lambda_{SC,N=6}$ and $\Lambda_{SC,N=11} = \Lambda_{SC,N=12}$. We also observe that the Λ_{SC} of Fig. 6 correspond to the smallest Λ at which a cluster of size N is shown to be stable in Fig. 2, if the softness of the HP and width of the potential well is correctly adjusted for. This is demonstrated in the SM §4 [29].

V. BREAKING THE DEGENERACY FOR $N = 5$

1. Simulation

The $N = 5$ spherical code has a continuum of solutions ranging from a square pyramid [Fig. 8(a)] to a triangular bipyramid [Fig. 8(b)]. For dense $N = 5$ clusters at nonzero temperature, we seek the relative likelihood of the cluster adopting particular configurations from the solution continuum. We construct an order parameter that can distinguish between different configurations in MC or BD simulations to facilitate this.

All $N = 5$ spherical code solutions have two points at opposite poles of the central sphere and differ by the positions of the three remaining points on the equator. The order parameter for an $N = 5$ cluster is constructed by first dividing the five HPs into "pole" HPs and "equator" HPs. The two HPs that are the farthest apart are designated the "pole" HPs

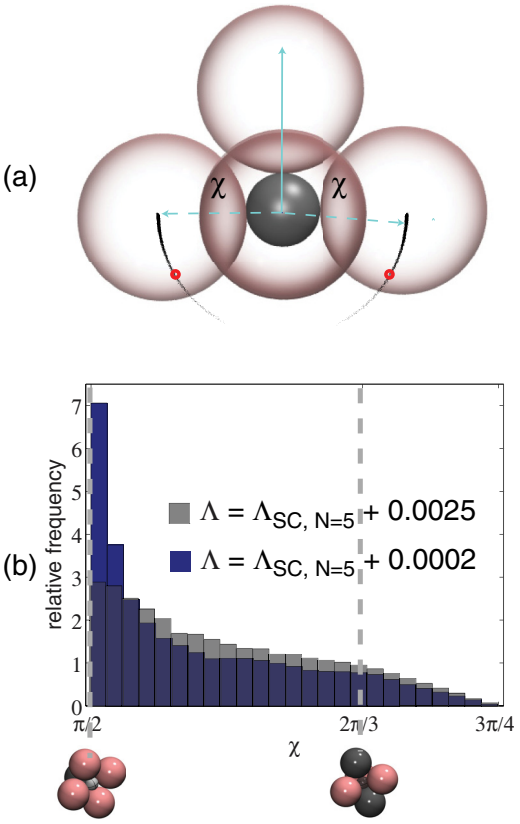

FIG. 7. (Color online) (a) Order parameter χ is constructed by measuring the angle of the particles on the equator. Scattered points from a simulation overlay an image of an SP configuration. Red circles indicate the sphere centers of a TBP configuration. In panel (b) the distribution of χ sampled from a Monte Carlo simulation is shown as a function of the diameter ratio $\Lambda = \Lambda_{SC,N=5} + 0.0025$ and $\Lambda_{SC,N=5} + 0.0002$, respectively.

[1]We use a subscript to indicate that Λ_{SC} is constant and not a dependent variable such as Λ or Λ^{BD}.

and the remaining HPs are the "equator" HPs. An equatorial plane is then constructed by fitting a plane to the centers of the three "equator" HPs and the center of the CP. The centers of the four spheres are then projected into the plane and the angles between vectors from the CP to the "equator" HPs are determined. The order parameter χ is then defined as the angles of this set, omitting the largest. Each angle pair uniquely specifies a configuration in the solution continuum. A perfect square pyramid configuration corresponds to two measurements of $\chi = \pi/2$ and a perfect triangular bipyramid configuration corresponds to two measurements of $\chi = 2\pi/3$ radians. Figure 7(a) illustrates how the order parameter was constructed, and shows a sampling of the HP positions in the equatorial plane from a simulation at $\Lambda^{BD} = 0.4$. The red circles correspond to the triangular bipyramid positions.

We performed MC simulations of hard spheres as Λ approaches $\Lambda_{SC,N=5}$ (at $\Lambda = \Lambda_{SC,N=5} + 0.0025$ and $\Lambda_{SC,N=5} + 0.0002$, respectively), shown in Fig. 7(b). Surprisingly, we find that the square pyramid is the preferred structure, even over the more symmetrical triangular bipyramid. As the cluster is packed denser, an even stronger preference for the square pyramid configuration over other configurations emerges. BD simulations confirm this preference, despite the softer model of the hard spheres (SM §5 [29]).

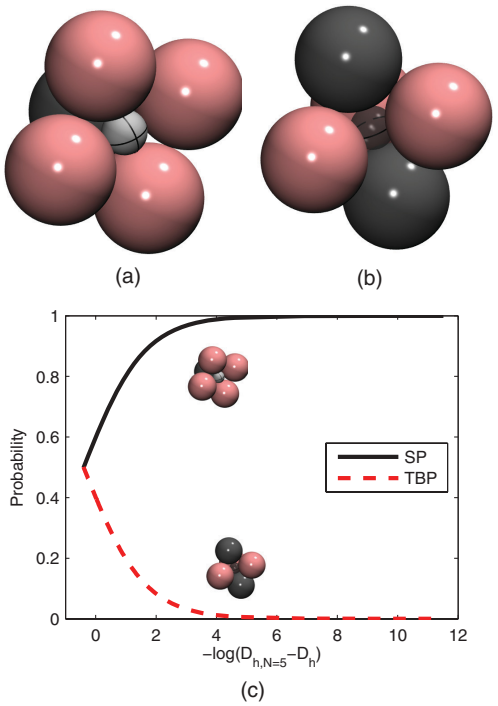

FIG. 8. (Color online) (a) Square pyramid (SP) and (b) triangular bipyramid (TBP) $N = 5$ spherical codes. The jammed and unjammed kissing spheres in each configuration are colored dark gray and pink, respectively. The path that the unjammed spheres can follow is traced on the central sphere. For panel (b) the central sphere is transparent so the full path around the equator can be seen. In the graph at the bottom, the preference for the SP (black solid) over the TBP (red solid) is evident as the HP diameter approaches the limiting packing diameter.

2. *Free energy*

To understand the entropic preference for the square pyramid configuration of the $N = 5$ cluster, we use a free energy calculation, which elucidates the role of entropy in breaking the degeneracy. The more symmetrical triangular bipyramid configuration is used as the reference configuration.

The square pyramid and triangular bipyramid HP clusters are shown in Figs. 8(a) and 8(b), respectively. In Fig. 8(c), using our free energy calculation, the probability of observing the square pyramid relative to the triangular bipyramid is shown as the HP diameter D_h approaches the diameter of spheres corresponding to the densest possible packing, $D_{h,N=5}$. According to this calculation, the square pyramid is always the most likely configuration. We find that this preference is due to the square pyramid having the most vibrational freedom, or free volume per particle. In Figs. 8(a) and 8(b), the locally unjammed HPs in a cluster at $\Lambda = \Lambda_{SC,N=5}$ are colored pink and the HPs that are locally jammed are colored gray. In the degenerate continuum of $N = 5$ spherical code solutions, only the square pyramid has only one locally jammed HP, and thus the highest vibrational freedom.

VI. DISCUSSION

By our choice of model and model parameters, diffusion of the HP on the surface of the CP is in no way penalized or restricted. In the temperature range we considered, the time τ_{bonded} that an HP remained bonded to a CP is much greater than the time $\tau_{\text{diffusion}}$ for an HP to explore the surface of the CP. If $\tau_{\text{diffusion}} \gg \tau_{\text{bonded}}$, (e.g., by lowering the diffusion rate of the HP on the surface of the CP), the structure of the cluster would instead resemble a different mathematical problem; namely, the random parking problem [38]. In this limit, the HPs are kinetically inhibited from finding their free-energy-minimizing state by long relaxation times. Schade *et al.* [39] experimentally and theoretically studied terminal colloidal clusters in this limit formed by electrostatics or DNA-mediated attraction.

However, when HP can freely diffuse on the CP surface, there are a number of ways the sticky sphere assembly method described above can be extended to create interesting new species of anisotropic particles.

A. Terminal cluster design from sphere surface extremal points

A more general question we can consider is, given a desired arrangement of points, what HP-CP interactions and HP-HP interactions will result in its self-assembly? The analogous mathematical question was posed by L. L. Whyte in 1952: "What spherical arrangements [of points] possess extremal properties of any kind?" [26] Ideally, we seek HP-HP interactions and HP-CP interactions that self-assemble repeatable and desirable patterns of HPs on the CP.

The problem of finding extremal points obtained by optimally distributing points on the surface of a sphere to minimize a function f has been well studied in the field of mathematics [25,26,40]. The problem is typically posed as follows:

Given N points on the surface of a sphere of radius R, what arrangement of the N points minimizes a function f?

If $f = k\sum_{i\neq j}^{N} r_{i,j}^{-n}$, where $r_{i,j}$ is the Euclidean distance between the points i and j, and $n = 1$, minimizing f corresponds to the Thomson problem, whose solution describes the distribution of identical point charges on the surface of a sphere. As $n \to \infty$, the problem corresponds to the spherical code problem. Other possible choices for f include minimizing the maximum distance of any point to its closest neighbor, also known as the *sphere covering problem*, and maximizing the volume of the convex hull of the points. For each of these problems solutions are exactly known for some values of N, while various numerical searches have suggested best solutions for other N. For the functions mentioned, tables of putative solutions up to at least $N = 130$ can be found in Ref. [24].

Cohn and Kumar [41] show that all potential energy functions of distance that are completely monotonic, such as inverse power laws, share a subset of universally optimal solution configurations. If the function is strictly monotonic, then the universally optimal solution is also unique. For points on the surface of a sphere, the only known universally optimal solutions are [41,42] $N = 1$–4, 6, and 12; that is, a single point, antipodal points, points forming an equilateral triangle on the equator, and tetrahedral, octahedral, and icosahedral arrangement of points. For our purposes, this means certain desired point arrangements (e.g., a ring of 12 points distributed around the equator of a sphere such as modeled in Ref. [43]) are likely to be inherently difficult to achieve from HP-HP interactions. Restricting themselves to isotropic pair potentials and identical particles, Cohn and Kumar [44] constructed separate decreasing convex potential energy functions that have cubic ($N = 8$) and dodecahedral ($N = 20$) configurations as their minimum. Thus, Refs. [41,42,44] imply that, to assemble certain clusters, it will be necessary to use more complicated HPs with carefully constructed potentials, including noncompletely monotonic or anisotropic interactions.

There may also be a correspondence between other mathematical sequences of points distributed on a sphere and terminal cluster assembly problems. For example, in Ref. [20,21] clusters of cones and clusters of spheres were shown to form unique and precisely packed clusters arising from free energy minimization subject to a convexity constraint. The authors find a packing sequence identical to that obtained from minimizing the second moment of the mass distribution of a cluster of particles constrained to a convex hull. We observe that the packing sequence produced in Ref. [20] also bears a strong resemblance to the distribution of points on the surface of a sphere that maximizes the convex hull [24]. The authors further showed that sequence successfully describes the polyhedral structures formed by colloidal spheres self-assembling on an evaporating droplet [12,13]. That work serves as another example of the correspondence between mathematical solutions of extremal points on the surface of a sphere and cluster structures obtainable in experiments.

Another interesting variant to consider is a nonspherical central particle, as was done in Ref. [45] for the Thomson problem. Considering the packing of HP around a nonspherical CP may lead to novel clusters and is a generally unexplored problem.

B. Terminal cluster design by staged assembly

Using an alternative approach, complex clusters may also be possible by simply adding stages to the assembly process. For example, if, after the terminal N-cluster of Fig. 1 is created, the bath of HPs is replaced by a bath of new HPs coated with the same complementary material as the CP, a second "shell" of spheres can be added to the first. The structure of this shell will also depend on the entropy and energy of the cluster at a given temperature. If the HPs in the second shell preferentially sit in the interstices of the first shell, the polyhedron they form will be the *dual* of the polyhedron of the first shell. This can make different types of point arrangements possible. For example, the dual of the octahedron is the cube. A cubic arrangement of eight points on the surface of a sphere is not found as a minimum among the most common spherical surface functions [24]. A second shell of HPs that preferentially assemble the dual of the first shell of HPs may be a physically more viable method of assembling a cubic arrangement of spheres without requiring the elaborately constructed HP-HP interaction potential of Cohn and Kumar [44].

VII. CONCLUSION

In this paper we have demonstrated that hard and sticky spheres can self-assemble into terminal N-clusters with interesting and, in some cases, unexpected, anisotropies. These clusters have predictable stable structures that depend on temperature and sphere diameter ratio.

If assembled directly from a bath at low temperature, certain cluster sizes (e.g., $N = 4, 6, 12$) form robustly, while other clusters occur only over small ranges with relatively mobile structures (e.g., $N = 7, 9, 10$) and still others cannot be formed at all (e.g., $N = 5, 11$). A "multistep" process can realize the hard-to-assemble clusters by beginning with assembly at high temperature, followed by removal of the HP bath and lowering the temperature. It may be possible to adjust the effective diameter of the HP or CP as a step in the assembly process. Our free energy calculations, Monte Carlo, and Brownian (molecular) dynamics predictions of cluster structure provide a guide for designing such a process for optimal yield of desired cluster sizes with a well-ordered structure. Clusters fabricated in this way may find use as building blocks for subsequent self-assembly, as templates for manufacturing precisely placed circular patches on the surface of a spherical particle and in the creation of nanocolloidal cages.

ACKNOWLEDGMENTS

We acknowledge Oleg Gang and Alexei Tkachenko for discussions of related problems. We acknowledge Daphne Klotsa for her helpful comments on the manuscript. C. L. P., M. M., and S. C. G. were supported by the US Department of Energy, Office of Basic Energy Sciences, Division of Materials Sciences and Engineering, under award DE-FG02-02ER46000. C. L. P. acknowledges support through a US Department of Energy Computational Science Graduate Fellowship. E. J. and S. C. G. received support from the James S. McDonnell Foundation 21st Century Science Research

Award/Studying Complex Systems, Grant No. 220020139 and E. J. received support from a National Defense Science and Engineering Graduate (NDSEG) Fellowship, 32 CFR 168a. S. C. G. is also supported by the DOD/DDRE under the National Security Science & Engineering Faculty Fellowship award No. N00244-09-1-0062.

[1] S. C. Glotzer and M. J. Solomon, Nat. Mater. **6**, 557 (2007).
[2] S. Sacanna and D. J. Pine, Curr. Opin. Colloid Interface Sci. **16**, 96 (2011).
[3] M. R. Jones, R. J. Macfarlane, B. Lee, J. Zhang, K. L. Young, A. J. Senesi, and C. A. Mirkin, Nat. Mater. **9**, 913 (2010).
[4] S. N. Fejer, D. Chakrabarti, and D. J. Wales, ACS Nano **4**, 219 (2010).
[5] S. N. Fejer, D. Chakrabarti, and D. J. Wales, Soft Matter **7**, 3553 (2011).
[6] A. J. Williamson, A. W. Wilber, J. P. K. Doye, and A. A. Louis, Soft Matter **7**, 3423 (2011).
[7] E. Jankowski and S. C. Glotzer, J. Phys. Chem. B **115**, 14321 (2011).
[8] E. Matijevic, Acc. Chem. Res. **14**, 22 (1981).
[9] K. Keville, E. Franses, and J. Caruthers, J. Colloid Interface Sci. **144**, 103 (1991).
[10] T. S. Ahmadi, Z. L. Wang, T. C. Green, A. Henglein, and M. A. El-Sayed, Science **272**, 1924 (1996).
[11] L. M. Liz-Marzán, M. Giersig, and P. Mulvaney, Langmuir **12**, 4329 (1996).
[12] V. N. Manoharan, M. T. Elsesser, and D. J. Pine, Science **301**, 483 (2003).
[13] E. Lauga and M. P. Brenner, Phys. Rev. Lett. **93**, 238301 (2004).
[14] Y.-S. Cho, G.-R. Yi, J.-M. Lim, S.-H. Kim, V. N. Manoharan, D. J. Pine, and S.-M. Yang, J. Am. Chem. Soc. **127**, 15968 (2005).
[15] Y.-S. Cho, G.-R. Yi, S.-H. Kim, M. T. Elsesser, D. R. Breed, and S.-M. Yang, J. Colloid Interface Sci. **318**, 124 (2008).
[16] L. Hong, A. Cacciuto, E. Luijten, and S. Granick, Nano Lett. **6**, 2510 (2006).
[17] D. Wales and J. Doye, J. Phys. Chem. A **101**, 5111 (1997).
[18] F. Sciortino, A. Giacometti, and G. Pastore, Phys. Chem. Chem. Phys. **12**, 11869 (2010).
[19] S. Mossa, F. Sciortino, P. Tartaglia, and E. Zaccarelli, Langmuir **20**, 10756 (2004).
[20] T. Chen, Z. Zhang, and S. C. Glotzer, Proc. Natl. Acad. Sci. USA **104**, 717 (2007).
[21] T. Chen, Z. Zhang, and S. C. Glotzer, Langmuir **23**, 6598 (2007).
[22] G. Meng, N. Arkus, M. P. Brenner, and V. N. Manoharan, Science **327**, 560 (2010).
[23] F. Tóth, *Regular Figures* (The Macmillan Company, 1964).
[24] N. J. A. Sloane, with the collaboration of R. H. Hardin, W. D. Smith, and others, *Tables of Spherical Codes, Coverings, Maximum Volume of Convex Hulls, and Minimal Energy Arrangements*, published electronically at www.research.att.com/~njas/.
[25] T. W. Melnyk, O. Knop, and W. R. Smith, Can. J. Chem. **55**, 1745 (1977).
[26] L. L. Whyte, Am. Math. Mon. **59**, 606 (1952).
[27] S. Sacanna, W. T. M. Irvine, P. M. Chaikin, and D. J. Pine, Nature (London) **464**, 575 (2010).
[28] C. P. Royall, W. C. K. Poon, and E. R. Weeks, Soft Matter (2012), doi:10.1039/c2sm26245b.
[29] See Supplemental Material at http://link.aps.org/supplemental/10.1103/PhysRevE.86.041124 for simulation and analysis details.
[30] D. J. McGinty, J. Chem. Phys. **55**, 580 (1971).
[31] R. J. Speedy, J. Chem. Soc., Faraday Trans. 2 **77** (1981).
[32] W. G. Hoover, N. E. Hoover, and K. Hanson, J. Chem. Phys. **70**, 1837 (1979).
[33] V. S. Kumar and V. Kumaran, J. Chem. Phys. **123**, 114501 (2005).
[34] S. S. Pablo, Frank, and H. Stillinger, Mol. Phys. **95**, 289 (1998).
[35] A. Haji-Akbari, M. Engel, and S. C. Glotzer, J. Chem. Phys. **135**, 194101 (2011).
[36] C. Phillips, E. Jankowski, and S. C. Glotzer, (unpublished).
[37] T. Aste and D. Weaire, *The Pursuit of Perfect Packing* (Institute of Physics Publishing, 2000).
[38] M. L. Mansfield, L. Rakesh, and D. A. Tomalia, J. Chem. Phys. **105**, 3245 (1996).
[39] N. B. Schade, M. C. Holmes-Cerfon, E. R. Chen, D. Aronzon, J. W. Collins, J. A. Fan, F. Capasso, and V. N. Manoharan, arXiv:1201.3952.
[40] J. R. Edmundson, Acta Crystallogr., Sect. A: Found. Crystallogr. **48**, 60 (1992).
[41] H. Cohn and A. Kumar, J. Amer. Math Soc. **20**, 99 (2007).
[42] B. Ballinger, G. Blekherman, H. Cohn, N. Giansiracusa, E. Kelly, and A. Schürmann, Exp. Math. **18**, 257 (2009).
[43] Z. Zhang and S. C. Glotzer, Nano Lett. **4**, 1407 (2004).
[44] H. Cohn and A. Kumar, Proc. Natl. Acad. Sci. USA **106**, 9570 (2009).
[45] G. Vernizzi and M. Olvera de la Cruz, Proc. Nat. Acad. Sci. **104**, 18382 (2007).